Transport rates of proteins in porous materials with known microgeometry

W. Mark Saltzman and Robert Langer
Harvard/MIT Division of Health Sciences and Technology and Department of Chemical Engineering, Massachusetts Institute of Technology, Cambridge, Massachusetts 02139

ABSTRACT Many biological and biotechnological systems involve the diffusion of macromolecules through complicated macroporous (pore size on the order of 10–100 μm) environments. In this report, we present and evaluate an experimental system for measuring the rate of protein transport in an inert, macroporous membrane. For this particular membrane system, the microgeometry was characterized in terms of distribution of pore size, position, and orientation. Although the rate of protein desorption was much less than expected based on continuum diffusion models, we demonstrate that the measured transport rates are consistent with diffusion of protein in a complex, interconnected network of water-filled pores. The porous systems exhibit transitional behavior in quantitative agreement with the behavior of percolation lattices (mean square error 7%, $n = 29$). Predictive mathematical models of the diffusion process were developed: these models used percolation concepts to describe pore topology, continuum models of diffusion/dissolution to describe protein movement at each single pore, and measured pore size distributions. Effective diffusion coefficients for protein transport in aqueous, constricted macropores were predicted by this technique. Predicted diffusion coefficients, based on measured and derived microstructural parameters, agree with experimentally measured diffusion coefficients within a factor of 2. This approach may be useful in the design of porous polymer systems for biological applications and for evaluating other biological systems where conduction of mass, heat, momentum, or charge occurs in a heterogeneous environment.

INTRODUCTION

The diffusion of molecules through a complex environment is encountered in many different physical systems. Much of the progress in developing descriptions of diffusion in heterogeneous materials has been made by physical scientists interested in geological materials (1), porous catalysts (2), or combustion (3). Diffusion in complicated environments also occurs in biological systems. For example, both endogenous molecules (e.g., hormones) and exogenous drugs must move through complicated extra- and intracellular environments before reaching their sites of action (4). Diffusion of proteins through porous polymer supports is an important consideration in the design of affinity chromatography or immobilized enzyme systems (5). In some biochemical systems, for example, drugs encapsulated in polymer membranes for subsequent implantation and controlled drug release (6), diffusion of molecules through a complicated environment determines the rate of the process (7, 8). Therefore, fundamental understanding of the rates of transport of molecules, particularly macromolecules, through porous materials would be useful in understanding in vivo situations and in developing novel biotechnological systems.

Molecular mechanisms, supported by mathematical models and experimental evidence, are already available for describing many distinct modes of diffusive transport through complex environments. For example, the movement of small molecules through dense polymer membranes (9), the hindered diffusion of small and large molecules through micropores (10–13), and the reptation of macromolecules in entangled polymer melts (14, 15) have been described. These modes of transport are appropriate for analyzing diffusion in certain biological systems, like pure lipid membranes or membranes with extremely narrow pores. Convincing descriptions do not yet exist for the diffusion of large molecules in a complicated macroporous environment. Therefore, in this report, diffusion of molecules through a macroporous material—inert and impermeable to the diffusing species—was considered.

To test mathematical models for the rates of transport of molecules in porous environments, transport rates were determined in a model system. Proteins were encapsulated in an ethylene-vinyl acetate copolymer (EVAc) matrix and subsequently released. Since they are biocompatible, these materials have been studied regarding their use as drug delivery vehicles (16–18). For the present work, EVAc/protein systems have several advantages: (*a*) the raw materials are inexpensive, (*b*) the composite

Dr. Saltzman's present address is Department of Chemical Engineering, The Johns Hopkins University, Room 42C, New Engineering Building, Baltimore, MD 21218.

Please address correspondence to R. Langer, MIT, E25-342.

0006-3495/89/01/163/09 $2.00

materials are easy to fabricate, (*c*) proteins are released from the membranes in large quantities permitting measurement without the use of radioisotopes, (*d*) the systems are reproducible with respect to release kinetics (17), (*e*) the membranes are durable, (*f*) rates of transport are adjustable over a wide range by changing simple fabrication parameters (17, 18), and (*g*) detailed microstructural properties of the material are measurable by direct visualization and image analysis (19). As we will describe, this last factor allows us to relate the transport rates to properties of the solute and measurable microstructural characteristics.

The study of diffusion in porous materials has been enhanced by the introduction of percolation theory (20). In this report, percolation concepts are used, together with a statistical description of pore structure, to describe the diffusion mechanism and develop an analytical expression for predicting diffusion rates. Predicted effective diffusion coefficients—based entirely on aqueous diffusion in the complicated pore geometry—agree with experimentally determined diffusion coefficients, supporting the proposed mechanism of protein transport. The work described in this paper establishes the feasibility of predicting mass transport rates for proteins in complex systems based on detailed descriptions of the microgeometry.

METHODS

Encapsulation of proteins in polymeric membranes

Macromolecule-enriched membranes were fabricated from EVAc copolymer with 40% vinyl acetate (Elvax 40P; DuPont Co., Wilmington, DE) and solid protein powder (BSA fraction V powder and bovine γ-globulin; Sigma Chemical Co., St. Louis, MO) by a previously reported solvent evaporation method (17). Briefly, the polymer was dissolved in methylene chloride to produce a 10% (wt/vol) solution. Protein powder was added to this solution in sufficient quantity to make the desired loading (mass % protein) in the final device. For each membrane system, the encapsulated protein powder, either albumin or γ-globulin, was sieved to large (150–250 μm) or small (45–75 μm) particle size before addition to the polymer solution.

The polymer/protein solution was cast on a level glass mold at dry ice temperature (~−80°C). The solvent was evaporated for 2 d at −20°C (760 mmHg) and an additional 2 d at room temperature under house vacuum (0.6 mmHg). After evaporation, thin disks were punched with a number 6 cork bore from the resulting slab. Each individual membrane had a thickness of ~0.1 cm and a diameter of 1.2 cm.

Release of proteins from polymeric membranes

For each molecular species and protein particle size, release was monitored for a series of loadings from 5 (protein weight %) to 50%. Each device was activated by immersion in 10 ml of sodium cacodylate buffer solution (21.4 g $Na(CH_3)_2AsO_2 \cdot 3H_2O$ and 27.0 ml 0.2 N HCl diluted to 1 liter, pH 7.4); the arsenic-containing buffer was used to inhibit bacterial growth in the aqueous solutions. To further discourage microcontamination, gentamicin sulfate was added at 0.2 g per liter after 500 cumulative hours of release. All experiments were performed at room temperature, ~25°C. At discrete time points, the supernatant buffer solution was completely replaced and the concentration of protein in the supernatant was determined by UV absorbance at 220 or 280 nm. Cumulative protein release versus time was tabulated by summing the mass of protein in the buffer at each time point. The solubility of each protein in the cacodylate buffer was determined by measuring the UV absorbance (at 220 nm) of the solution phase of a saturated solution.

Determination of membrane microstructure

The pore structure of each of these materials was quantified by computer-assisted video light microscopy; details have been previously reported (19). Average properties (porosity, surface to volume ratio, mean pore size, and extent of pore orientation) and distributions (pore size and pore position) were determined.

MODEL DEVELOPMENT

For a homogeneous cylindrical slab (thickness $L \ll$ radius R), desorption of encapsulated molecules can be described by the one-dimensional form of Fick's second law:

$$\frac{\partial C}{\partial t} = D\frac{\partial^2 C}{\partial x^2}, \tag{1}$$

where C is the concentration of diffusing solute and D is the diffusion coefficient for the solute in the slab. Assuming a uniform initial distribution of solute in the slab ($C = C_0$ at $t = 0$, $-L < x < L$) and perfect sink conditions at the slab boundaries ($C = 0$ at $x = \pm L$, $t > 0$), the solution to Eq. 1 is (21)

$$\frac{C_0 - C}{C_0} = 1 - \frac{4}{\pi}\sum_{n=0}^{\infty}\frac{(-1)^n}{(2n+1)}\exp\left[\frac{-D(2n+1)^2\pi^2 t}{4L^2}\right] \cdot \cos\left[\frac{(2n+1)\pi x}{2L}\right]. \tag{2}$$

Upon integration of Eq. 2, the fraction of initially incorporated solute released at any time, F_t, is found:

$$F_t = \frac{M_t}{M_o} = 1 - \sum_{n=0}^{\infty}\frac{1}{(2n+1)^2\pi^2} \cdot \exp\left[\frac{-D(2n+1)^2\pi^2 t}{4L^2}\right], \tag{3}$$

where M_t is the cumulative mass of solute desorbed at time t and M_0 is the mass of solute initially contained within the slab. For a homogeneous slab, where the diffusion coefficient is constant throughout the material, all of the solute initially contained within the slab is eventually released ($F_t \rightarrow 1$ as $t \rightarrow \infty$).

In many porous materials, solute diffuses only through a water-filled pore space and is excluded from the material backbone. Therefore, the diffusion coefficient is a function of microscopic location in the slab:

$$D(\mathbf{x}) = \begin{cases} D_0 \text{ when } \mathbf{x} \text{ is in the pore space} \\ 0 \text{ when } \mathbf{x} \text{ is in the material,} \end{cases} \quad (4)$$

where D_0 is the diffusion coefficient of the solute in water and the vector $\mathbf{x}$ defines a site in the three-dimensional material. An exact solution then requires integration of Fick's second law over the completely characterized three-dimensional pore structure of the material. Alternatively, this complexity can be reduced by considering semi-empirical modifications of Eq. 1, as discussed below.

For inhomogeneous systems, one-dimensional desorption of solute from the porous slab can be described by the expression (22)

$$\frac{\partial(\epsilon C)}{\partial t} = \frac{\partial}{\partial x}\left(\epsilon D_{\text{eff}} \frac{\partial C}{\partial x}\right). \quad (5)$$

In the absence of restricted diffusion, the effective diffusion coefficient is defined (10, 22)

$$D_{\text{eff}} = \frac{D_0}{\tau}, \quad (6)$$

where τ is the tortuosity. Tortuosity is frequently interpreted as the fractional increase in diffusional path length due to the presence of impenetrable, immobile barriers in the material. When defined as in Eq. 6, τ also includes the effect of pore shape, pore connectivity, and, in an average sense, physical properties of the solute. For materials with a uniform distribution of porosity (ϵ is a constant in the slab: $-L < x < L$), Eq. 5 reduces to

$$\frac{\partial C}{\partial t} = D_{\text{eff}} \frac{\partial^2 C}{\partial x^2}, \quad (7)$$

and the solution to this equation for a porous slab is identical to Eq. 2 with the substitution of D_{eff} for D. The integrated expression for F_t is identical to Eq. 3 with the substitution of D_{eff} for D. In this case, however, F_t is equal to M/M_∞, where M_∞ is the mass of solute that is eventually released. As discussed in the paragraphs below, for materials with low porosity ($\epsilon < 0.3$), M_∞ can be significantly less than M_0. In the remainder of this section, we describe methods for estimating the fraction of solute desorbed, M_∞/M_0, and the effective diffusion coefficient, D_{eff}, based on microstructural characteristics of the porous material.

Percolation theory can be used to describe the diffusion of mass in porous systems (20, 23). Consider a porous material consisting of discrete regions of a conducting phase dispersed in an insulating phase. For simplicity, we will refer to the discrete conducting regions as pores. For such a material, provided that the material is infinite in extent, a sharp change in conductivity is observed at some critical porosity (volume fraction of conducting phase) (24). This critical porosity value, which is dependent on the lattice topology, marks the formation of an infinite (or material spanning) cluster of connected pores. Only pores that are members of this infinite cluster are accessible from the exterior of the material.

Many real materials cannot be assumed infinite in extent. When the material is finite, pores initially containing solute can transport mass to the surface if they extend to a single exterior face: the cluster of pores need not be material spanning to conduct. The case of finite materials, not uncommon for biological materials, is not well treated in the current literature.

For a porous material of finite extent the fraction of accessible porosity has two contributions: (*a*) from pores in the infinite cluster and (*b*) from pores in clusters of finite size that are coincident with the material boundary. The fraction of pores in the infinite cluster is equal to the fraction of accessible porosity in a material of infinite extent, ϵ_a. This quantity is a function of the total porosity, ϵ, and the pore lattice topology, usually characterized by a lattice coordination number ζ. Fig. 1 shows the variation of ϵ_a with ϵ for an arbitrary lattice. Below some threshold value the volume of the infinite cluster is zero; above the threshold, the fraction of accessible porosity grows with total porosity.

Finite clusters of pores are classified according to the number of connected pores in the cluster, n. Cluster size distributions in a percolation lattice are described by a cluster distribution function, s_n: the volume fraction of clusters containing n member pores. For a given cluster size, s_n is a function of ϵ and ζ. In a finite material, large clusters have a greater probability of contacting the material surface than small clusters: the probability that a cluster of size n contacts the surface, $p_v(nv^*)$, is a function of total cluster volume nv^*, where v^* is the mean pore volume. Therefore, the total fraction of accessible porosity—with contributions from finite and infinite pore clusters—is given by

$$\epsilon_a^T = \frac{M\infty}{M_0} = \epsilon_a(\epsilon, \zeta) + \sum_{n=1}^{\infty} s_n(n, \epsilon, \zeta)\, p_v(nv^*), \quad (8)$$

where $\epsilon_a^T = a$ is the total fraction of accessible pore volume in the material. Due to the contribution from finite-size pore clusters (right-hand term in Eq. 8), accessible porosity is non-zero below the threshold value, as shown in Fig. 1. For desorption of a solute from a porous material, the fraction of accessible porosity is equal to the fraction of initial solute that desorbs after a long time, M_∞/M_0.

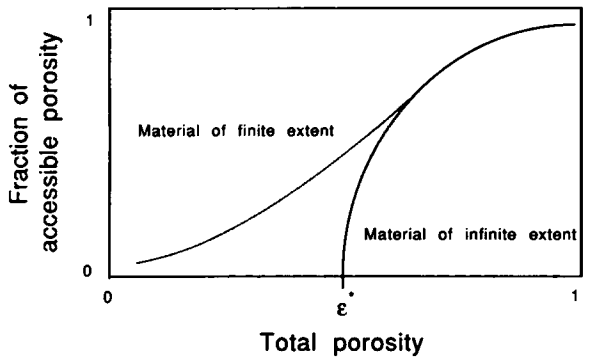

FIGURE 1 Fraction of accessible porosity for materials of infinite and finite extent. For infinite materials, the fraction of accessible porosity is zero below the percolation threshold ϵ^*. For finite materials, the fraction of accessible porosity can be nonzero at all porosities, due to pore clusters of finite size located near the material surface.

To use Eq. 8 for predicting the fraction of accessible porosity, a specific percolation lattice structure must be chosen. Lattice structures can be probabilistic (e.g., Voronoi tesellations [25]), ordered (e.g., cubic or triangular lattices [24]), or idealized (e.g., Bethe lattice [26–28]). A commonly used structure is the Bethe lattice, a homogeneous tree-like structure. Each Bethe lattice has a central site and ζ initial branches; the site on the end of each new branch has $\zeta - 1$ of its own branches, and so on. This resulting structure has a coordination number ζ. Although the Bethe lattice is idealized, cluster size distributions (27) and effective conductivities (28) can be predicted analytically upon assumption of ζ. For example, the cluster size distribution for a Bethe lattice is given by

$$s_n(n, \epsilon, \zeta) = \frac{2(\zeta - 1)[(n + 1)(\zeta - 1) - 1]!}{(n - 1)![(n + 1)(\zeta - 1) - n + 1]!} \cdot \epsilon^n (1 - \epsilon)^{(\zeta-2)n+\zeta}. \quad (9)$$

Conductivities and cluster size distributions in other, more physically realistic, lattices, usually obtained by Monte Carlo simulation, can be analytically approximated by an equivalent Bethe lattice (20, 23, 25, 26).

Consider a porous material—surrounded by an aqueous phase—where the pores initially contain concentrated, or solid, solute. During desorption of the water soluble solute, there are two potential sources for local retardation of the diffusive flux: (*a*) retardation due to dissolution and concentration dependent diffusion of solute molecules, and (*b*) retardation due to the porous environment. Assuming that these effects are independent, the effective diffusion coefficient is given by

$$D_{\text{eff}} = D_0 f(C_0, C_S) h[\epsilon, \zeta, L(X)], \quad (10)$$

where D_{eff} is the effective diffusion coefficient of a solute in the polymer pore space, D_0 is the diffusion coefficient of the solute in water, $f(C_0, C_s)$ is the effect of solute physical properties, and $h[\epsilon, \zeta, L(X)]$ is the effect of pore geometry. The effect of solute physical properties depends on the solubility C_s and the initial solute concentration in the pore space C_0. The effect of pore geometry depends on porosity ϵ, lattice topology ζ, and the rate of solute movement between adjacent pores (i.e., the pore-to-pore transport rate) $L(X)$, where X is some characteristic parameter of an individual pore (e.g., pore diameter). Since pores in the material have a distribution of size and shape, $L(X)$ has a distribution of values. By assuming that the effects of solute properties and pore geometry are independent, $f(C_0, C_s)$ can be determined by considering continuum diffusion models for solute transport in each water-filled pore and $h[\epsilon, \zeta, L(X)]$ can be determined by analyzing diffusion from pore-to-pore on a percolation lattice.

Two physical properties of the solute are potentially important in limiting the rate of mass transport through the porous material: concentration dependence of the diffusion coefficient and a finite rate of solute dissolution in the pore space. These properties were considered most significant because (*a*) diffusion coefficients of proteins are known to be a function of concentration (29) and (*b*) proteins are highly soluble in water. Other potential sources for retardation of the diffusion flux (e.g., hindered diffusion, electrostatic interactions, and adsorption/desorption to polymer surfaces) were not considered important for this analysis (see Discussion). For these two effects, $f(C_0, C_s)$ can be determined by solutions to Fick's second law with (*a*) moving boundary of dissolution (30, 31) and (*b*) concentration-dependent diffusion coefficients (29, 32). Solution of Fick's law in these cases usually requires a numerical method; an effective diffusion coefficient for the numerical solution, D^n_{eff}, is estimated by comparison of the numerical solution with Eq. 3. The effect of solute physical properties, $f(C_0, C_s)$, is then equal to D^n_{eff}/D_0.

For a Bethe lattice with coordination number ζ, the effective conductivity due to pore geometry can be determined analytically (23, 28):

$$h[\epsilon, \zeta, L(X)] = -\frac{\zeta - 1}{\zeta - 2}\frac{C'(0)}{D_0}, \quad (11)$$

where $C'(0)$ is defined by the integral equation

$$\int_0^\infty e^{-tx} C(x)dx = \int_0^\infty G[L(X)] \left\{ \frac{1}{t + L(X)} + \frac{L^2(X)}{[t + L(X)]^2} \int_0^\infty \exp\left[-\frac{L(X)t}{L(X) + t} x \right] C(x)^{\zeta-1} dx \right\} dL(X), \quad (12)$$

where t is a transform variable, $G[L(X)]$ is a normalized probability distribution of transport rates through indi-

vidual pores, and $C(0) = 1$. Methods for solving this integral equation are available (28).

In this report, we examined EVAc/protein materials with a wide range of initial mass fraction protein: 5 to 50%. By quantifying the total fraction of protein desorbed from these membranes as a function of total porosity, we gain insight into the nature of pore clustering in the composite material. That insight is used as a basis for predicting protein transport rates in the porous polymer. We confine our examination of effective diffusion coefficients to materials above the percolation threshold, where Eq. 10 is valid.

RESULTS

To test this description of diffusion in a macroporous material, solid particles of protein—BSA and γ-globulin—were encapsulated in EVAc copolymer membranes. Upon activation by immersion in aqueous buffer solution, protein was slowly released from the ~1-mm thick membranes for a period of over 1 yr (Fig. 2). For membranes with low initial concentration of protein, protein was trapped in the material. This is shown clearly in Fig. 2 where the total fraction of protein released is determined from the asymptotic value of the fraction released versus time. Both the rate of release of protein and the total fraction of releasable protein depended on several parameters: the initial mass fraction of protein in the membrane (Fig. 2 *a*), the size of the encapsulated particles (Fig. 2 *b*), and the macromolecular species (Fig. 2 *c*). The rate of protein release also depended on the thickness of the membrane (data not shown).

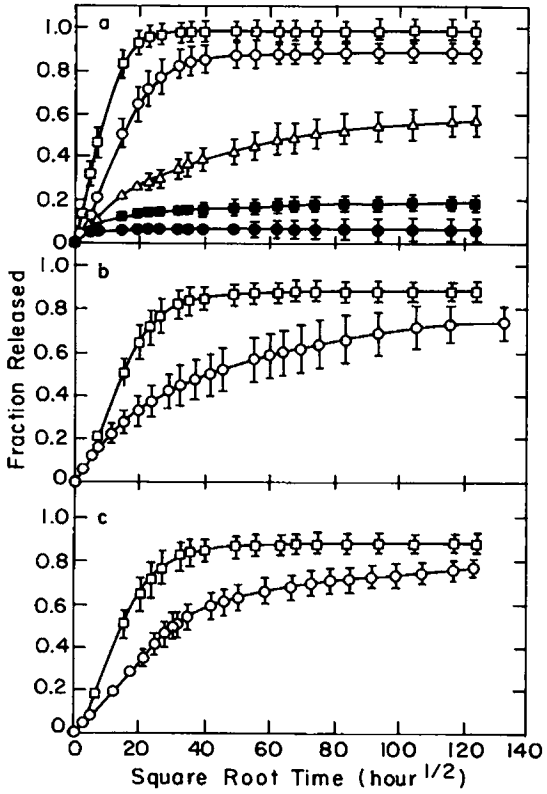

FIGURE 2 Fraction of protein released is plotted versus the square root of time. In *a*, the initial mass fraction of protein in the membrane was 50% (□), 40%, (○), 30% (△), 20% (■), and 5% (●) BSA. In *b*, large 150–250 μm (□) and small 45–75 μm (○) particles of BSA were encapsulated at a protein mass fraction of 40%. In *c*, the macromolecular species of the 150–250-μm particle encapsulated powder was BSA (□) or γ-globulin (○) at 40% mass fraction. Points indicate the mean and the error bars indicate the standard deviation of five devices; where not shown error bars are smaller than symbol.

To relate microscopic models of local transport to a bulk system, the pore structure of the protein/polymer membranes was quantified using cryomicrotomy and image analysis. The results have appeared previously (19), so we summarize them here. Microscopic observations revealed a continuous polymer phase; uniformly dispersed in this continuous phase were discrete pores filled with solid protein. Porosity and surface to volume ratio were determined from microscopic sections at various positions ($-L < x < L$) within the membrane. Regression analysis revealed no significant variation in porosity or surface to volume ratio through the polymer matrix. Individual pores exhibited no preferred axis of orientation in the membranes. The initial concentration of protein in the pores of each membrane was calculated from the experimentally determined porosity, known mass fraction of protein in the membrane, and the known density of pure polymer; numerical values are given in Table 1. The pore size distribution was approximately bimodal: large diameter pores (>10–30 μm) occupied ~90% of the particle volume fraction while the majority of pores, by number, had small diameters (<10–30 μm); pore size distributions have been reported previously (19,

TABLE 1 Properties of polymer/protein membranes

	BSA		γ-Globulin
	150–250-μm Particles	45–75-μm Particles	150–250-μm Particles
C_0 (g/cm³)	1.1	1.1	1.2
C_S (g/cm³)	0.59	0.59	0.30
$f(C_0, C_S)$	0.27	0.27	0.14
ν^* (cm³)	9.2×10^{-6}	1.2×10^{-6}	6.8×10^{-6}

Values for initial protein concentration in the pore space (C_0, calculated as previously described [19]), protein solubility (C_S, measured in supernatant of a saturated solution), mean pore volume (ν^*, measured by image analysis), and the effect of solute physical properties on the diffusion coefficient $f(C_0, C_S)$ (calculated as described in the text) are shown for the three different protein/polymer systems.

33). Mean pore volumes for each set of membranes are given in Table 1. Microscopic sections cut perpendicular to the large surface area face of the membrane (i.e., perpendicular to the $x = \pm L$ planes) were examined to determine the distribution of pore position. The observed distributions of pore center position were uniform across the membrane (34).

Since the polymer is inert and impermeable to the encapsulated solute (35), pore diffusion should be the only transport mechanism. Indeed, the release curves shown in Fig. 2 were initially linear with respect to the square root of time suggesting that these materials follow this paradigm. In fact, the release curves presented in Fig. 2 can be represented by two parameters, the effective diffusion coefficient D_{eff} and the fraction of protein released M_∞/M_0. Experimental values for D_{eff} were determined by comparing the release curves (as shown in Fig. 2) to continuum expressions for desorption from a finite slab; numerical values are presented in Table 2. Experimental values of M_∞/M_0 were determined from the asymptote of the release curves. As previously reported (18, 36) and confirmed here, the experimentally determined effective diffusion coefficient was orders of magnitude smaller than the diffusion coefficient of the protein in water. We now demonstrate that diffusion of macromolecules in a constricted macroporous environment, as described by Eqs. 8 and 10, is consistent with these measured rates.

The similarity of the results to percolation processes is apparent from the sharp increase in release rate and total fraction of protein released that occurs at ~30% initial mass fraction protein. Experimental values of the total fraction of BSA or γ-globulin released from EVAc membranes versus total porosity in the material are shown in Fig. 3; solid lines indicate the fraction of accessible porosity predicted by Eq. 8. Mean pore volume and total porosity were determined by image analysis; $p_v(n\upsilon^*)$ was the probability that a cluster of average radius $\frac{1}{2}\sqrt[3]{n\upsilon^*}$ contacted the membrane edge when uniformly distributed; $\epsilon_a(\epsilon, \zeta)$ and $s_n(n, \epsilon, \zeta)$ were estimated by assuming an effective coordination number (Eq. 9). For these predictions, a single effective coordination number was chosen based on the transition behavior of the experimental curves; the experimentally observed critical porosity p_c fixed the effective coordination number for a Bethe lattice as $1/(\zeta - 1) = p_c$ (27). Since the inflection points in the experimental curves were close to 0.33, an effective coordination number of 4 was selected to define the pore network topology. As seen in Fig. 3, the experimental values agree with this simple model of percolation behav-

TABLE 2 Measured effective diffusion coefficients (cm^2/s) for protein desorption

	BSA		γ-Globulin
	150–250-μm Particles	45–75-μm Particles	150–250-μm Particles
5%	3.3×10^{-11} (21,000)	— (—)	1.0×10^{-11} (44,000)
20%	9.5×10^{-11} (7,400)	1.3×10^{-11} (55,000)	1.0×10^{-11} (44,000)
30%	1.1×10^{-10} (6,600)	1.0×10^{-11} (68,000)	4.6×10^{-11} (9,500)
40%	8.1×10^{-10} (870)	4.5×10^{-10} (1,600)	9.5×10^{-11} (4,600)
50%	4.6×10^{-9} (150)	1.4×10^{-9} (500)	9.1×10^{-10} (481)

Each diffusion coefficient was determined by comparing the initial slope of the release curve—like the ones shown in Fig. 2—to Eq. 3. Tortuosity values are shown in parentheses; these were calculated by dividing the aqueous diffusion coefficient for the protein (7.0×10^{-7} cm^2/s for BSA and 4.4×10^{-7} cm^2/s for γ-globulin) by the experimentally determined effective diffusion coefficient.

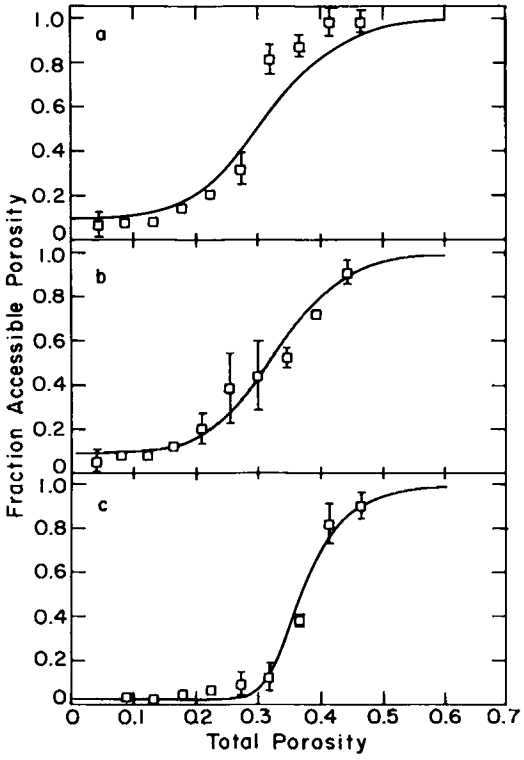

FIGURE 3 The total fraction released is plotted versus the total membrane porosity (volume fraction of material occupied by protein particles) for three different membrane systems: (*a*) large particle BSA, (*b*) large particle GAM, and (*c*) small particle BSA. Total porosity for each membrane was determined by image analysis (19). Points represent mean and standard deviation for five membranes. Solid lines indicate the model prediction from Eq. 5 assuming a Bethe lattice topology ($\zeta = 4$).

ior. For this prediction, only ζ was chosen; all the other parameters in Eq. 8 were measured.

This same lattice topology, Bethe lattice with coordination number 4, was used to predict the effective diffusion coefficient in the polymer pore space (Eq. 10). Since the initial concentration of protein in the pore space and the protein solubility were known, the effect of finite solubility in the pore space, $f(C_0, C_s)$, was predicted using continuum moving boundary models and analytical expressions for the dependence of protein diffusion coefficient on concentration. First, given an initial protein concentration and solubility in the pore space, Fick's second law was solved for the case of a moving boundary of dissolution (30, 31). An effective diffusion coefficient due strictly to finite solubility, D^1_{eff}, was determined by comparison with Eq. 3 (details are provided elsewhere [34]). Second, an experimentally determined expression for the concentration dependent diffusion coefficient of albumin (22) was used to calculate an effective diffusion coefficient due strictly to high concentrations, D^2_{eff}; the form of this expression was assumed valid for both albumin and γ-globulin. The method for calculation of D^2_{eff}, involving solution of Fick's second law with a nonconstant diffusion coefficient, has been previously described (32). Finally, $f(C_0, C_s)$ was calculated as $D^1_{eff} D^2_{eff}/D_o$; numerical values are given in Table 1.

The effect of pore geometry, $h[\epsilon, \zeta, L(X)]$, was calculated as follows; details are available (34). The observed bimodal distribution was separated into two distributions, $f_r(r)$ and $g_R(R)$: the first distribution describing small connecting pore channels and the second distribution describing macropores formed by the encapsulated solute particles (6, 37). A distribution of the ratio of adjacent pore radii, $j_X(X)$ where $X = r/R$, was derived from these two distributions by standard methods (38). For diffusion through constricted spherical pores, individual transport coefficients were calculated from a previously derived analytical expression (39):

$$L(X) = D_0 \frac{2X + \cos\theta}{\frac{2X}{\sin^2\theta} + a_w(\theta)}, \qquad (13)$$

where $\theta = \sin^{-1}(X)$, $a_w = [A(\theta) + 1 - \cos^3\theta]/\sin^2\theta$, and $A(\theta)$ is a series of Legendre polynomials (39). Since the distribution of pore radii $j_x(X)$ was known, the distribution of transport coefficients followed directly from Eq. 13. Finally, the effect of pore geometry, $h[\epsilon, \zeta, L(X)]$, was calculated based on a Bethe lattice topology ($\zeta = 4$) by substituting the calculated distribution of transport coefficients into Eqs. 11 and 12 and solving the integral equation (23, 28).

Predicted effective diffusion coefficients are compared to experimentally determined effective diffusion coefficients in Fig. 4. The effective diffusion coefficient, predicted by Eq. 10, is in good agreement with the experimentally determined effective diffusion coefficient. For a wide range of material properties, the assumption of a Bethe lattice topology yields an accurate prediction.

DISCUSSION

Effective diffusion coefficients were predicted by assuming, based on evidence obtained from quantitative image analysis (19), that two populations of pores were present in the porous membranes. While most of the solute resided in large pores comprising 90% of the pore space, many small pores were also apparent. We have previously shown that these small pores form constricted channels between the larger pores (6, 27). When considering protein diffusion at a local site in the pore space, the ratio of the large pore radius to adjacent small pore radius determines the local rate of mass transport.

The effective diffusion coefficient for protein transport in a complex porous environment can be approximated by this method. The method contains no adjustable parameters; ζ was chosen based on the observed percolation threshold of the system. Since the method is an approximation, several limitations are worth mentioning:

(*a*) In describing the connectivity of the pore network, a simple Bethe lattice model was employed. The Bethe lattice model was selected because (*i*) it is one of the few

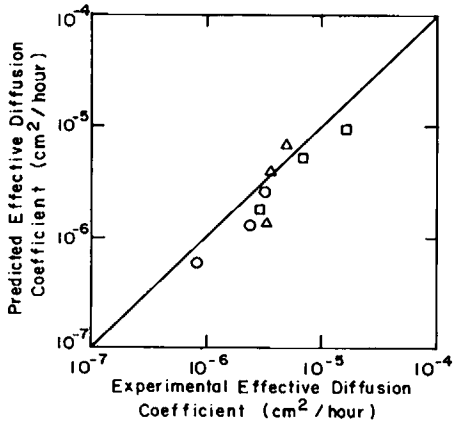

FIGURE 4 The predicted values of effective diffusion coefficient are compared to estimated values from experimental data for 150–250-μm particle BSA (□), 150–250-μm particle GAM (○), and 45–75-μm particle BSA (△). Experimental effective diffusion coefficients were obtained by comparing release curves (as in Fig. 2, see Table 2 for numerical values) to continuum expressions for desorption from a finite slab. Predicted effective diffusion coefficients were calculated as described in the text. Bethe lattice topology with an effective coordination number ($\zeta = 4$) was assumed for all calculations.

lattice topologies that permits an analytical description of its important cluster properties, and (*ii*) the properties of more physically realistic lattices can be approximated by assuming a Bethe lattice topology with an effective coordination number. An effective coordination number of 4 for the Bethe lattice was suitable for describing the transition behavior of these porous systems (Fig. 3). This does not imply that the average coordination number for pores in the polymer matrix is 4. Determination of the actual coordination number and topology of the pore network in the porous polymer matrices requires a three-dimensional reconstruction of the entire matrix. We are currently developing methods for reconstruction and determination of the lattice topology.

(*b*) The effects of finite solubility, concentration dependence of the aqueous diffusion coefficient, pore geometry, and lattice topology were assumed independent. An exact description of protein diffusion in the porous network would consider all of these effects simultaneously. For example, the diffusion equation could be written in the polymer pore space with a concentration-dependent diffusion coefficient, a moving boundary of dissolution at the solid/liquid interface, and a complete description of the pore geometry as boundary conditions for protein diffusion. This requires a three-dimensional description of the entire pore network and a sophisticated numerical method for including the complex boundary conditions. The good agreement of predicted and measured diffusion coefficients provided by this approximate approach (Fig. 4) justifies its use until more complete models of the three-dimensional pore microgeometry are available.

(*c*) Hindered diffusion of protein was not considered because of the relatively large size of the smallest element in the pore network (~10 μm). In other systems, where the pore size approaches the diameter of the diffusing molecule, this effect can be included by modification of Eq. 10:

$$D_{\text{eff}} = D_0 f(C_0, C_S)\, h[\epsilon, \zeta, L(X)]\, K_r(\lambda), \qquad (14)$$

where λ is the ratio of solute radius to pore radius. The function $K_r(\lambda)$, the effect of hindered or restricted diffusion on the free solution diffusion coefficient, has been experimentally measured for a number of different macromolecules (10–13). In this approximation, the pore-to-pore transport rates are modified by hindered diffusion in pores of sufficiently small radius. Electrostatic effects could be approximated in a similar manner.

(*d*) Adsorption/desorption of proteins to the polymer surface were not considered. Experimentally measured surface-to-volume ratios in the polymer suggested that the maximum amount of protein which could be absorbed to the polymer surface was less than 0.1% of the total encapsulated protein (19). In other systems, where the concentration of protein in the pore space is lower, adsorption/desorption phenomena may play an important role in determining the transport rates. For these cases, the mechanism of the surface phenomena must be known and, in general, an approach which explicitly considers the relative rates of adsorption and diffusion adopted. As a first approximation the rate of adsorption and desorption can be compared to the rate of diffusive transport predicted by this method and, when the rates are comparable, the resistances may be added in series.

(*e*) The polymer matrix pore structure was assumed static throughout the period of protein desorption. In fact, as water enters the constricted polymer pore space, the pore structure may change due to the viscoelastic nature of the EVAc polymer and the high osmotic pressure of concentrated protein solutions (40). In our case, the experimentally measured desorption curves were well described by a constant effective diffusion coefficient. If the pore structure were changing dramatically, the effective diffusion coefficient of protein in the polymer pore space would be a function of time. Therefore, we believe that dynamic changes in the pore structure will have a small effect on protein transport rates. We are currently developing methods for observing the polymer pore structure at times after immersion in buffer. These methods will be useful for applying our analysis to other materials, like erodible or swellable polymers, where significant changes in the pore structure are known to occur.

CONCLUSION

These results support a purely diffusion mechanism for protein transport through macroporous polymers. They also establish the feasibility of predicting transport rates of macromolecules in complex porous membranes by detailed microstructural modelling with percolation theory. The assumption of a Bethe lattice topology permits an analytical method for predicting transport rates in the porous polymer. Since Bethe lattice topologies predict the same transition and effective conductivity behavior as several more realistic topologies, we suspect that inclusion of a more realistic topology will have little impact on the predictions. Although employed here to describe transport in an inert polymeric membrane, we expect that this approach can be adapted to describe conduction processes in many macroporous materials. While the formulation strictly applies only to two phase materials where the dispersed phase is a perfect insulator, it can be used in concert with descriptions of other diffusive transport mechanisms (9–15) to explore more complicated materials, such as the release of encapsulated solutes from degrading or hydrophilic polymers and the transport of

proteins across biological barriers, where more than one transport mechanism is important.

We thank Dr. Norman Sheppard and Prof. Ronald Siegel for useful discussions.

This work was supported by the National Science Foundation.

Received for publication 29 April 1988 and in final form 15 September 1988.

REFERENCES

1. Scheidegger, A. E. 1970. The Physics of Flow Through Porous Media. University of Toronto Press, Toronto.
2. Satterfield, C. N. 1970. Mass Transport in Heterogeneous Catalysis. MIT Press, Cambridge, MA.
3. Froment, G. F., and K. B. Bischoff. 1979. Chemical Reaction Analysis and Design. John Wiley & Sons, New York.
4. Christensen, H. N. 1975. Biological Transport. 2nd ed., WA Benjamin Inc., Reading, MA.
5. Bernstein, H., V. C. Yang, and R. Langer. 1987. Distribution of heparinase covalently immobilized to agarose: experimental and theoretical studies. *Biotechnol. Bioeng.* 30:196–207.
6. Siegel, R. A., and R. Langer. 1984. Controlled release of polypeptides and other macromolecules. *Pharm. Res.* 1:2–10.
7. Siegel, R. A., and R. Langer. 1986. A new Monte Carlo approach to diffusion in constricted porous geometries. *J. Coll. Interface Sci.* 109:426–440.
8. Balazs, A. C., D. F. Calef, J. M. Deutch, R. A. Siegel, and R. Langer. 1985. The role of polymer matrix structure and interparticle interactions in diffusion-limited drug release. *Biophys. J.* 47:97–104.
9. Leib, W. R., and W. D. Stein. 1969. Biological membranes behave as non-porous polymeric sheets with respect to diffusion of non-electrolytes. *Nature (Lond.).* 224:240–243.
10. Satterfield, C. N., C. K. Colton, and W. H. Pitcher. 1973. Restricted diffusion in liquids within fine pores. *AIChE J.* 19:628–635.
11. Renkin, E. M. 1954. Filtration, diffusion, and molecular sieving through porous cellulose membranes. *J. Gen. Physiol.* 38:225.
12. Anderson, J. L., and J. A. Quinn. 1974. Restricted transport in small pores. A model for steric exclusion and hindered particle motion. *Biophys. J.* 14:130–150.
13. Deen, W. M. 1987. Hindered transport of large molecules in liquid-filled pores. *AIChE J.* 33:1409–1425.
14. Klein, J. 1978. Evidence for reptation in an entangled polymer melt. *Nature (Lond.).* 271:143–145.
15. DeGennes, P. G. 1971. Reptation of a polymer chain in the presence of fixed obstacles. *J. Chem. Phys.* 55:572–579.
16. Langer, R., and J. Folkman. 1976. Polymers for the sustained release of proteins and other macromolecules. *Nature (Lond.).* 263:797–799.
17. Rhine, W. D., D. S. T. Hsieh, and R. Langer. 1980. Polymers for sustained macromolecule release: procedures to fabricate reproducible delivery systems and control release kinetics. *J. Pharm. Sci.* 69:265–270.
18. Miller, E. S., and N. A. Peppas. 1983. Diffusional release of water-soluble bioactive agents from ethylene-vinyl acetate copolymers. *Chem. Eng. Commun.* 22:79–92.
19. Saltzman, W. M., S. H. Pasternak, and R. Langer. 1987. Quantitative image analysis for developing microstructural descriptions of heterogeneous materials. *Chem. Eng. Sci.* 42:1989–2004.
20. Mohanty, K. K., J. M. Ottino, and H. T. Davis. 1982. Reaction and transport in disordered composite media: introduction of percolation concepts. *Chem. Eng. Sci.* 37:905–924.
21. Crank, J. 1975. The Mathematics of Diffusion. 2nd ed., Oxford Press, New York, 47.
22. Bhatia, S. K. 1986. Stochastic theory of transport in inhomogeneous media. *Chem. Eng. Sci.* 41:1311–1324.
23. Reyes, S., and K. F. Jensen. 1985. Estimation of effective transport coefficients in porous solids based on percolation concepts. *Chem. Eng. Sci.* 40:1723–1734.
24. Kirkpatrick, S. 1973. Percolation and conduction. *Rev. Mod. Phys.* 45:574–588.
25. Winterfeld, P. H., L. E. Scriven, and H. T. Davis. 1981. Percolation and conduction of random two-dimensional composites. *J. Phys. C.* 14:2361–2376.
26. Larson, R. G., L. E. Scriven, and H. T. Davis. 1981. Percolation theory of residual phases in porous media. *Nature (Lond.).* 268:409–413.
27. Fisher, M. E., and J. W. Essam. 1961. Some cluster size and percolation problems. *J. Math. Phys.* 2:609–619.
28. Stinchcombe, R. B. 1974. Conductivity and spin-wave stiffness in disordered systems. *J. Phys. C.* 7:170–203.
29. Keller, K. H., E. R. Canales, and S. I. Yum. 1971. Tracer and mutual diffusion coefficients of proteins. *J. Phys. Chem.* 75:379–387.
30. Paul, D. R., and S. K. McSpadden. 1976. Diffusional release of a solute from a polymer matrix. *J. Membr. Sci.* 1:33–48.
31. Danckwerts, P. V. 1950. Unsteady-state diffusion or heat conduction with moving boundaries. *Trans. Faraday Soc.* 46:701–722.
32. Siegel, R. A., 1984. Macromolecular Drug Release from Porous Implants: Sources of Matrix Tortuosity. Ph.D. thesis, Massachusetts Institute of Technology, Cambridge, MA.
33. Saltzman, W. M., S. H. Pasternak, and R. Langer. 1987. Microstructural models for diffusive transport in porous polymers. *ACS Symp. Ser.* 348:16–33.
34. Saltzman, W. M. 1987. A microstructural approach for modelling diffusion of bioactive macromolecules in porous polymers. Ph.D. thesis, Massachusetts Institute of Technology, Cambridge, MA.
35. Hsu, T. T., and R. Langer. 1985. Polymers for the controlled release of macromolecules. *J. Biomed. Materials Res.* 19:445–460.
36. Bawa, R., R. A. Siegel, B. Marasca, M. Karel, and R. Langer. 1985. An explanation for the controlled release of macromolecules from polymers. *J. Controlled Release.* 1:259–267.
37. Siegel, R. A., J. Kost, and R. Langer. 1989. Mechanistic studies of macromolecular drug release from macroporous polymers. I. Experiments and preliminary theory concerning completeness of release. *J. Controlled Release.* In press.
38. Drake, A. W. 1967. Fundamentals of Applied Probability Theory. McGraw-Hill, New York.
39. Ballal, G., and K. Zygourakis. 1985. Diffusion in particles with pores of varying cross-section. *Chem. Eng. Sci.* 40:1477–1483.
40. Vilker, V. L., C. K. Colton, and K. A. Smith. 1981. The osmotic pressure of concentrated protein solutions: effect of concentration and pH in saline solutions of bovine serum albumin. *J. Coll. Surface Sci.* 79:548–566.